Nuclear Engineering and Technology 54 (2022) 4215–4219

Contents lists available at ScienceDirect

Nuclear Engineering and Technology

journal homepage: www.elsevier.com/locate/net

Original Article

Growth and characterization of detector-grade CdMnTeSe

J. Byun [a, b], J. Seo [a, b], J. Seo [a, b], B. Park [a, b, *]

[a] Dept. of Health and Safety Convergence Science, Korea University, Seoul, 02841, South Korea
[b] Interdisciplinary Program in Precision Public Health, Korea University, Seoul, 02841, South Korea

ARTICLE INFO

Article history:
Received 19 April 2022
Received in revised form
29 May 2022
Accepted 7 June 2022
Available online 12 June 2022

Keywords:
CdMnTeSe
Vertical bridgman technique
Radiation detector
Characterization

ABSTRACT

The $Cd_{0.95}Mn_{0.05}Te_{0.98}Se_{0.02}$ (CMTS) ingot was grown by the vertical Bridgman technique at low pressure. All wafers showed high resistivity, which suggests potential as a room-temperature semiconductor detector. The resistivity of the CMTS planar detector was 1.47×10^{10} Ω· cm and mobility lifetime product of electrons was 1.29×10^{-3} cm^2/V. The spectroscopic property with Am-241 and Co-57 was evaluated. The energy resolution about 59.5 keV gamma-ray of Am-241 was 11% and the photo-peak of 122 keV gamma-ray from Co-57 was clearly distinguished. The result shows the first detector-grade CMTS in the world and proves CMTS's potential as a radiation detector operating at room temperature.

1. Introduction

X- and gamma-ray detectors are needed in aerospace, medical imaging, security, and high energy physics [1–4]. Many candidates of X- and gamma-ray detectors operate at room temperature (i.e., thallium bromide [5], mercuric iodide [6], perovskite [7], and cadmium telluride-based semiconductor [8,9]). The most successful material is cadmium zinc telluride ($Cd_{0.9}Zn_{0.1}Te$) which is commercially developed by some vendors. However, CdZnTe has some problems with Te inclusions, the sub-grain boundary, and the segregation coefficient of zinc [10–13].

Recently, Roy [14–16] reported on the role of selenium in the CdTe matrix or CdZnTe materials. The addition of selenium in the CdTe matrix results in improved compositional uniformity and reduced defects (dislocation, subgrain boundary) [15]. Additionally, our team recently reported the PL spectra of CdZnTeSe to show that the addition of 2% selenium to the CdZnTe materials can improve the crystalline and eliminate the defect level of 1.1 eV [17]. Meanwhile, the addition of manganese in CdTe could solve the problem from the segregation coefficient of zinc, because of manganese's more stable segregation property ($k = 1$ in the CdTe matrix). It allows a higher yield of detectors in CdMnTe than in CdZnTe, meaning a reduction in cost and production of large-volume detectors with homogeneity [9,18,19]. Thus, CdMnTeSe is an ideal material with which the challenging problems of the CdTe-based materials could be solved. In this experiment, CdMnTeSe crystals were grown using the vertical Bridgman technique, fabricated to the planar dimension, and investigated.

2. Experiment

The $Cd_{0.95}Mn_{0.05}Te_{0.98}Se_{0.02}$ (CMTS) ingot with a 2-inch diameter was grown by the vertical Bridgman technique at low pressure as shown in Fig. 1. Precursors were stoichiometric amounts of CdTe(6N), Mn(6N), Te(7N), CdSe(5N), and a few ppm of indium. The growth and synthesis were done in the carbon-coated quartz crucible. The purpose of carbon-coating is to prevent thermal damage from the difference in thermal expansion coefficient between the quartz and CMTS. A series of processes for growing ingot was carried out in a vacuum of less than 2×10^{-6} Torr at room temperature. The sealed crucible was taken into a vertical furnace and heated to 1120∘C for 5 h and kept for 12 h. Super heating and super cooling were not adopted. A temperature profile was set to avoid the occurrence of Te precipitate. The temperature gradients for growth and dropping speed were, respectively, 5-10 K/cm and 2.5 mm/h. The ingot was cooled down to room temperature for 3 days.

The grown ingot was perpendicularly sliced to wafers every 6.5 mm thickness using a diamond wire saw. Then, specimens with the same physical dimension were extracted from each wafer to calculate resistivity related to the position in the ingot. Specimens with planar dimensions were made from the middle wafer which

* Corresponding author. Dept. of Health and Safety Convergence Science, Korea university, Seoul, 02841, South Korea.
E-mail address: pbj0116@korea.ac.kr (B. Park).

https://doi.org/10.1016/j.net.2022.06.007
1738-5733/

had the highest resistivity. The cut crystals were mechanically lapped with sandpaper and polished with an Al_2O_3 abrasive up to 0.3 μm. The chemical treatment with Br-based etchant was done and followed by deposition using an $AuCl_3$ solution and passivation with an ammonium fluoride passivant [20].

The leakage current was measured using Keithley 237 source measure unit with a range from -300 to 300 V. The spectroscopic property was taken with Am-241 and Co-57 irradiated to the cathode side of the detector. The signals generated from the 59.5 keV gamma-ray were obtained from the positively biased anode electrode. The mobility-lifetime product ($\mu\tau_e$) was calculated by Hecht' equation fitting [21,22]. Components for spectroscopic measurement were CRZ-110 preamplifier (Cremat Inc.), CR-200 shaping amplifier (Cremat Inc.), Easy-MCA-8k (Amptek), and Ortec 659 power supply. The shaping time of all measurements was 2 μs. Measurements of the current-voltage curve and pulse height spectra were done under 25∘C to exclude temperature-induced effects.

3. Results and discussion

The Bridgman-grown CMTS ingot was sliced into wafers and entitled from 1 to 9, corresponding with their order from tip to heel. In each wafer, planar samples were extracted to measure the electrical property of the wafers. The samples were fabricated in the same physical dimension. Au electrodes were then deposited on both sides of the samples with a fixed size. The leakage current of each sample was measured in the range of -50 to 50 V. Fig. 2 shows the resistivity of the planar samples, which was calculated with the measured leakage current. Wafers 1 and 9 were excluded from the result as were respectively tip and heel. Wafer 4 shows the highest resistivity among the specimens. The segregation coefficient of indium dopant in the CdTe matrix differed depending on concentration but was normally within 0.2 [23,24]. The amount of indium increases from tip to heel while CMTS maintains its stoichiometric property because of the uniform segregation coefficient of manganese and selenium [9,25]. Thus, the resistivity of the CMTS wafer was determined by the position related to the amount of indium. Among CMTS wafers, wafer 4 is closest to the charge neutrality compensated by the amount of indium.

The planar CMTS samples from wafer 4 were made with a series of fabrications. The samples were treated with the 2% Br-MeOH solution and passivants following mechanical lapping and polishing. The electroless deposition was conducted on both sides of the samples to evaluate the transport property, resistivity, and pulse height spectrum. Fig. 3 shows the dark current of the representative sample at the applied bias ranging from -300 to 300 V. The I-V characteristic represents an almost perfect linear curve, indicating the formation of ohmic contact [26]. The calculated resistivity of the sample was $1.47 \times 10^{10}\ \Omega \cdot \mathrm{cm}$ less than that of CdMnTe in previous research [9,27]. The other CMTS samples from the same wafer had similar values of resistivity, possibly from the selenium reducing the band gap of material in the CdTe matrix [28]. The resistivity decreases with a decreasing band gap when assuming the full compensation; however, the resistivity of our samples exceeds the requirement ($>10^9\ \Omega \cdot \mathrm{cm}$) for a semiconductor detector operating

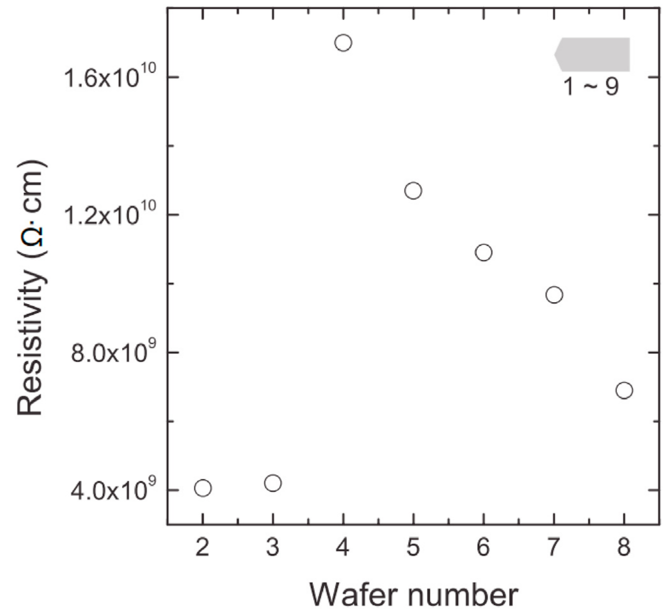

Fig. 2. Resistivity of wafers sliced from the CMTS ingot.

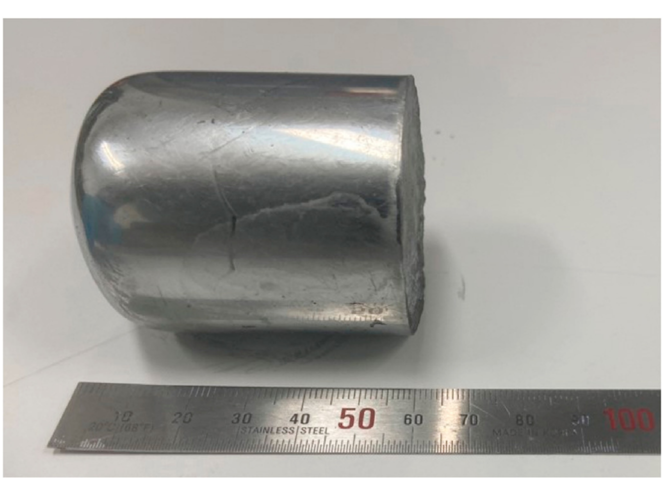

Fig. 1. Photograph of the $Cd_{0.95}Mn_{0.05}Te_{0.98}Se_{0.02}$:In ingot grown by. the vertical Bridgman technique at low pressure.

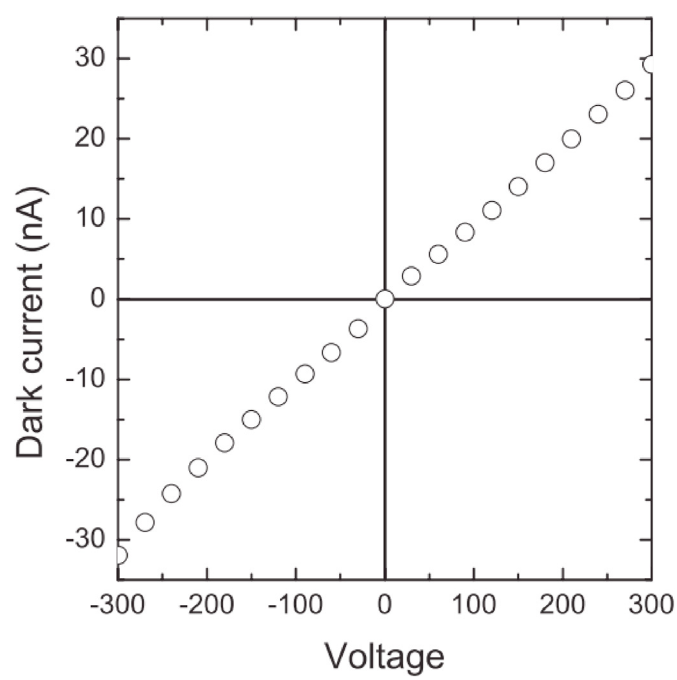

Fig. 3. Dark current of the planar CMTS sample ranging from -300 to 300 V.

at room temperature.

$\mu\tau_e$ is an important parameter to evaluate the transport property of a semiconductor detector. A $\mu\tau_e$ of more than 10^{-3} cm^2/V without additional annealing is normally considered for radiation detector operating at room temperature and could be calculated with Hecht's equation below, Where L is detector thickness, Q is the collected charge [21].

$$CCE = \frac{Q}{Q_0} = \frac{\mu\tau_e E}{L}\left[1 - exp\left(-\frac{L}{\mu\tau_e E}\right)\right] \quad (1)$$

$\mu\tau_h$ is excluded because of its little path of hole when low-energy gamma-rays are irradiated to the cathode. what to summarize the equation (1) as equation for Q and to replace the E as V/L is the modified Hecht's equation below [22].

$$Q = Q_0\frac{\mu\tau_e V}{L^2}\left[1 - exp\left(-\frac{L^2}{\mu\tau_e V}\right)\right] \quad (2)$$

$\mu\tau_e$ can be calculated with equation (2), when putting peak centroid and bias voltage into Q and V, respectively. The response of CMTS irradiated by 59.5 keV gamma-rays of Am241 radioisotope was measured at various bias voltages. Positions of peak at each voltage were recorded, which is proportional to charge collection efficiency. The data were fitted with equation (2) and the result is shown in Fig. 4. The obtained $\mu\tau_e$ value is 1.29×10^{-3} cm^2/V, making the as-grown CMTS a good candidate for a room-temperature semiconductor detector.

Fig. 5 represents the spectroscopic property of the planar CMTS detector about 59.5 keV gamma-rays of Am-241. A 240 V was applied, at which point the leakage current of the CMTS detector was about 20 nA as shown in Fig. 3. The energy resolution of 59.5 keV photo-peak is 11%, and the peak of Np L X-ray is also well distinguished. The spectroscopic property of the CMTS was serviceable, However, the photo-peak of 59.5 keV is not a perfect Gaussian shape because of the hole tail on the left side of the photo-peak.

This hole's effect is more easily observed in the spectrum of Co-57 in Fig. 6. The measurement conditions of Co-57 were the same as previously. The main energy of Co-57 gamma-rays is 122 keV which has a lower attenuation coefficient to CMTS than 59.5 keV gamma-rays of Am-241 [29], thereby causing the large variation of penetrating depth. The interaction point determines the path length of the carriers generated from the incident gamma-ray. A different path length influences the collection of holes because of low $\mu\tau_h$,

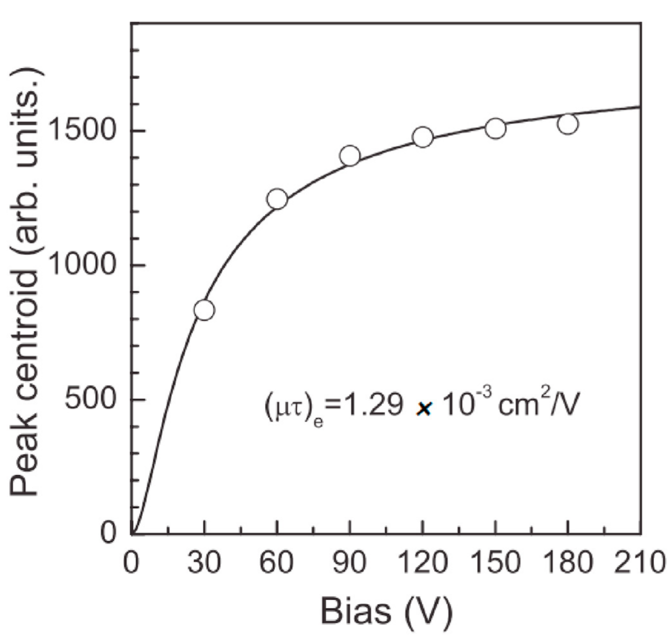

Fig. 4. A plot of peak centroid of 59.5 keV gamma-ray versus bias. voltage. The mobility-lifetime product of electrons was calculated to fit the experimental. data (open circuit) with Hecht's equation [22].

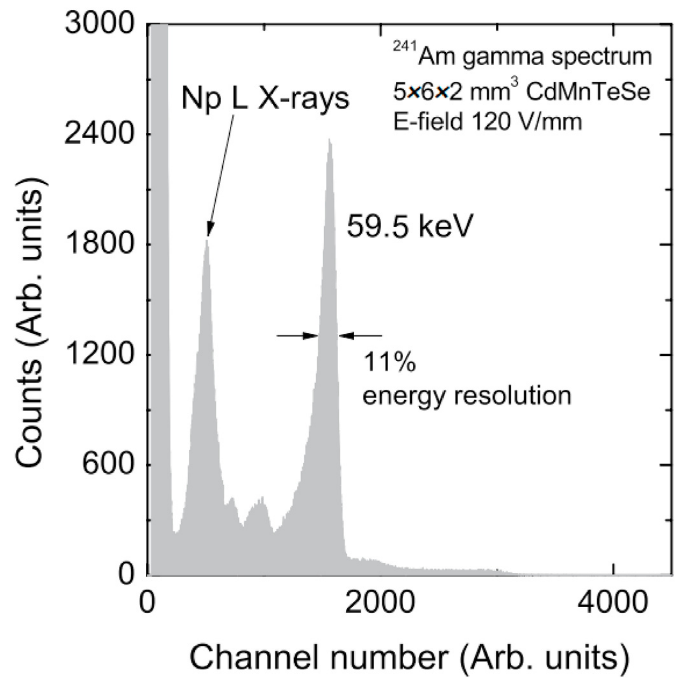

Fig. 5. Pulse height spectrum of planar CMTS detector irradiated by. Am-241. The energy resolution at 59.5 keV gamma-rays of Am-241 was 11%.

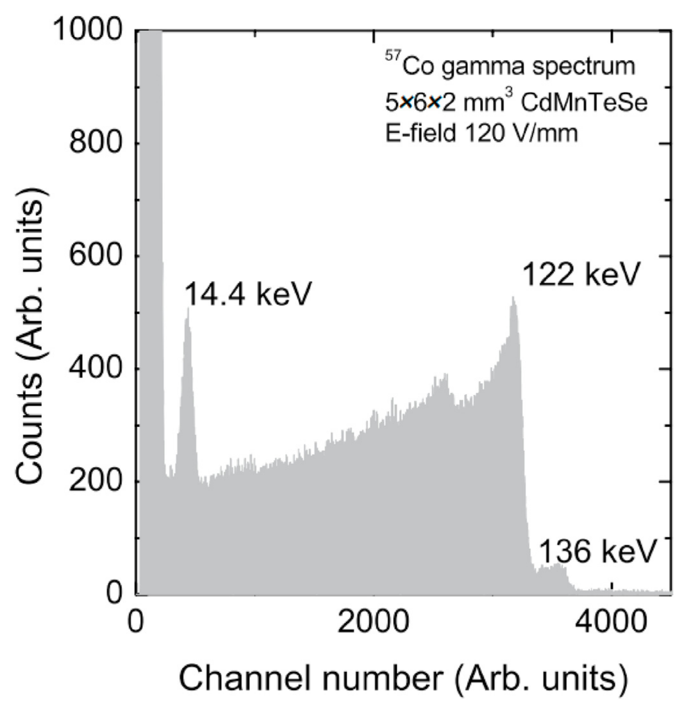

Fig. 6. Pulse height spectrum of planar CMTS detector irradiated by Co-57. The effect of incomplete charge appears.

while rarely influencing the collection of the electron. In Fig. 6 all gamma-ray peaks are distinguished and accompanied by the charge loss from the incomplete charge [30]. Thus, the CMTS detector needs more improvements to be used as a room-temperature semiconductor detector.

The hole's low charge collection can be explained in two ways. First, degradation originates from precursor impurities. The raw CdSe had a 5N purity, which is lower than that of other materials (6~7N). Previous research [25] states that the different results of electrical property were observed during the several growths of CdZnTeSe due to the specific impurities of CdSe. Second, Te inclusions reduce the performance of CdTe-based semiconductor detectors [31]. Roy [32] stated that the addition of selenium in the CdTe matrix could reduce the concentration of Te inclusions. But the outbreak of Te inclusion originated from the locked-up melt of CdZnTe grown by the Bridgman technique and traveling heater method [33,34]. It is hard to explain the reduction of Te inclusion corresponds with the addition of selenium; therefore, grown CMTS might also be influenced by Te inclusions. Using of CdSe with a higher purity and two-step annealing [35,36] can enhance performance of the CMTS detectors.

4. Summary

CMTS is a good candidate for a gamma-rays detector. Moreover, CMTS is free from the segregation of zinc because it is replaced with manganese. This study confirmed that CMTS can operate at room temperature with good electrical, transport, and spectroscopic properties. The potential of CMTS as a detector might be additionally enhanced with an increase in the purity of raw materials and the two-step annealing process.

Declaration of competing interest

The authors declare that they have no known competing financial interests or personal relationships that could have appeared to influence the work reported in this paper.

Acknowledgments

This work was supported by the National Research Foundation of Korea (NRF) grant funded by the Korea government (MSIT) (No. 2021R1A2C1012161), by Ministry of Environment as "the Graduate school of Particulate matter specialization" and by Korea Institute of Energy Technology Evaluation and Planning (KETEP) grant funded by the Korea government (MOTIE) (20214000000070, Promoting of expert for energy industry advancement in the field of radiation technology).

References

[1] R.B. James, T.E. Schlesinger, J. Lund, M. Schieber, Semiconductors and Semimetals Semiconductors for Room Temperature Nuclear Detector Applications, Elsevier, New York, 1995.

[2] S. Watanabe, H. Tajima, Y. Fukazawa, Y. Ichinohe, S. Takeda, T. Enoto, T. Fukuyama, S. Furui, K. Genba, K. Hagino, A. Harayama, Y. Kuroda, D. Matsuura, R. Nakamura, K. Nakazawa, H. Noda, H. Okada, M. Ohta, M. Onishi, S. Saito, G. Sato, T. Sato, T. Takahashi, T. Tanaka, A. Togo, S. Tomizuka, The Si/CdTe semiconductor Compton camera of the ASTRO-H soft gamma-ray detector (SGD), Nucl. Instrum. Meth. A. 765 (2014) 192–201, https://doi.org/10.1016/j.nima.2014.05.127.

[3] K. Iniewski, CZT detector technology for medical imaging, J. Instrum. 9 (11) (2014), C11001, https://doi.org/10.1088/1748-0221/9/11/c11001.

[4] A. Burger, M. Groza, Y. Cui, U.N. Roy, D. Hillman, M. Guo, L. Li, G.W. Wright, R.B. James, Development of portable CdZnTe spectrometers for remote sensing of signatures from nuclear materials, Phys. Status. Solidi. A. C2 (2005) 1586–1591, https://doi.org/10.1002/pssc.200460839.

[5] K. Hitomi, T. Onodera, T. Shoji, Influence of zone purification process on TlBr crystals for radiation detector fabrication, Nucl. Instrum. Meth. A. 579 (1) (2007) 153–156, https://doi.org/10.1016/j.nima.2007.04.028.

[6] A. Kargar, E. Ariesanti, S. James, D.S. McGregor, Charge collection efficiency characterization of a HgI_2 Frisch collar spectrometer with collimated high energy gamma rays, Nucl. Instrum. Meth. A. 652 (1) (2011) 186–192, https://doi.org/10.1016/j.nima.2010.08.057.

[7] Y. He, M. Petryk, Z. Liu, D.G. Chica, I. Hadar, C. Leak, W. Ke, I. Spanopoulos, W. Lin, D. Chung, B.W. Wessels, Z. He, M.G. Kanatzidis, $CsPbBr_3$ perovskite detectors with 1.4 % energy resolution for high-energy γ-rays, Nat. Photonics. 15 (1) (2021) 36–42, https://doi.org/10.1038/s41566-020-00727-1.

[8] H. Shiraki, M. Funaki, Y. Ando, A. Tachibana, S. Kominami, R. Ohno, THM growth and characterization of 100 mm diameter CdTe single crystals, IEEE Trans. Nucl. Sci. 56 (4) (2009) 1717–1723, https://doi.org/10.1109/TNS.2009.2016843.

[9] K. Kim, S. Cho, J. Suh, J. Hong, S. Kim, Gamma-ray response of semi-insulating CdMnTe crystals, IEEE Trans. Nucl. Sci. 56 (3) (2009) 858–862, https://doi.org/10.1109/TNS.2009.2015662.

[10] A.E. Bolotnikov, N.M. Abdul-jabbar, O.S. Babalola, G.S. Camarda, Y. Cui, A.M. Hossain, E.M. Jackson, H.C. Jackson, J.A. James, K.T. Kohman, A.L. Luryi, R.B. James, Effects of Te inclusions on the performance of CdZnTe radiation detectors, IEEE Trans. Nucl. Sci. 55 (5) (2008) 2757–2764, https://doi.org/10.1109/TNS.2008.2003355.

[11] A.E. Bolotnikov, G.S. Camarda, Y. Cui, G. Yang, A. Hossain, K. Kim, R.B. James, Haracterization and evaluation of extended defects in CZT crystals for gamma-ray detectors, J. Cryst. Growth 379 (2013) 46–56, https://doi.org/10.1016/j.jcrysgro.2013.01.048.

[12] N. Zhang, A. Yeckel, A. Burger, Y. Cu, K.G. Lynn, J.J. Derby, Anomalous segregation during electrodynamic gradient freeze growth of cadmium zinc telluride, J. Cryst. Growth 325 (1) (2011) 10–19, https://doi.org/10.1016/j.jcrysgro.2011.04.041.

[13] P. Rudolph, M. Manfred, Basic problems of vertical Bridgman growth of CdTe, Mater. Sci. Eng. B. 16 (1-3) (1993) 8–16, https://doi.org/10.1016/0921-5107(93)90005-8.

[14] U.N. Roy, G.S. Camarda, Y. Cui, R. Gul, A. Hossain, G. Yang, J. Zazvorka, V. Dedic, J. Franc, R.B. James, Role of selenium addition to CdZnTe matrix for room-temperature radiation detector applications, Sci. Rep. 9 (1) (2019) 1–7, https://doi.org/10.1038/s41598-018-38188-w.

[15] U.N. Roy, G.S. Camarda, Y. Cui, R. Gul, G. Yang, J. Zazvorka, V. Dedic, J. Franc, R.B. James, Evaluation of CdZnTeSe as a high-quality gamma-ray spectroscopic material with better compositional homogeneity and reduced defects, Sci. Rep. 9 (1) (2019) 1–7, https://doi.org/10.1038/s41598-019-43778-3.

[16] U.N. Roy, G.S. Camarda, Y. Cui, R.B. James, High-resolution virtual Frisch grid gamma-ray detectors based on as-grown CdZnTeSe with reduced defects, Appl. Phys. Lett. 114 (23) (2019), 232107, https://doi.org/10.1063/1.5109119.

[17] B. Park, Y. Kim, J. Seo, J. Byun, J. Dedic, J. Franc, A.E. Bolotnikov, R.B. James, K. Kim, Bandgap engineering of $Cd_{1-x}Zn_xTe_{1-y}Se_y$ (0< x< 0.27, 0< y< 0.026, Nucl. Instrum. Meth. A. (2022), 166836, https://doi.org/10.1016/j.nima.2022.166836.

[18] S.U. Egarievwe, E.D. Lukosi, R.B. James, U.N. Roy, J.J. Derby, Advances in CdMnTe nuclear radiation detectors development, in: 2018 IEEE Trans. Nucl. Sci. Conf. R, 2018, https://doi.org/10.1109/NSSMIC.2018.8824694.

[19] U.N. Roy, G.S. Camarda, Y. Cui, R. Gul, A. Hossain, G. Yang, O.K. Okobiah, S.U. Egarievwe, R.B. James, Growth of CdMnTe free of large Te inclusions using the vertical Bridgman technique, J. Cryst. Growth 509 (2019) 35–39, https://doi.org/10.1016/j.jcrysgro.2018.12.026.

[20] G.W. Wright, R.B. James, D. Chinn, B.A. Brunett, R.W. Olsen, J. Van Scyoc, M. Clift, A. Burger, K. Chattopadhyay, D. Shi, R. Wingfield, Evaluation of NH_4F/H_2O_2 effectiveness as a surface passivation agent for $Cd_{1-x}Zn_xTe$ crystals, Proc. SPIE 4141 (2000) 324, https://doi.org/10.1117/12.407594.

[21] K. Hecht, Zum Mechanismus des lichtelektrischen Primärstromes in isolierenden Kristallen, Z. Phys. 77 (3-4) (1932) 235–245, https://doi.org/10.1007/BF01338917.

[22] R. Mats, M. Weidner, Charge collection efficiency and space charge formation in CdTe gamma and X-ray detectors, Nucl. Instrum. Meth. A. 406 (1998) 287, https://doi.org/10.1016/S0168-9002(98)91988-X.

[23] K. Yokota, H. Nakai, K. Satoh, S. Katayama, Segregation coefficients and activation of indium in cadmium telluride grown from tellurium-rich melt by the Bridgman technique, J. Cryst. Growth 112 (4) (1991) 723–728, https://doi.org/10.1016/0022-0248(91)90127-Q.

[24] P. Fochuk, O. Panchuk, P. Feychuk, L. Shcherbak, A. Savitskyi, O. Parfenyuk, M. Ilashchuk, M. Hage-Ali, P. Siffert, Indium dopant behaviour in CdTe single crystals, Nucl. Instrum. Meth. A. 458 (1-2) (2001) 104–112, https://doi.org/10.1016/S0168-9002(00)00926-8.

[25] S. Hwang, H. Yu, A.E. Bolotnikov, R.B. James, K. Kim, Anomalous Te inclusion size and distribution in CdZnTeSe, IEEE Trans. Nucl. Sci. 66 (2019) 2329, https://doi.org/10.1109/TNS.2019.2944969.

[26] Q. Li, W. Jie, L. Fu, X. Wang, X. Zhang, Metal–CdZnTe contact and its annealing behaviors, Appl. Surf. Sci. 253 (3) (2006) 1190–1193, https://doi.org/10.1016/j.apsusc.2006.01.058.

[27] Y. Du, W. Jie, T. Wang, T. Xu, L. Yin, P. Yu, G. Zha, Vertical Bridgman growth and characterization of CdMnTe crystals for gamma-ray radiation detector, J. Cryst. Growth 318 (1) (2011) 1062–1066, https://doi.org/10.1016/j.jcrysgro.2010.11.086.

[28] M. Lingg, A. Spescha, S.G. Haass, R. Carron, S. Buecheler, A.N. Tiwari, Structural and electronic properties of $CdTe_{1-x}Se_x$ films and their application in solar cells, Sci. Technol. Adv. Mater. 19 (1) (2018) 683–692, https://doi.org/

10.1080/14686996.2018.1497403.
[29] https://www.nist.gov/pml/x-ray-mass-attenuation-coefficients.
[30] Y. Eisen, Y. Horovitz, Correction of incomplete charge collection in CdTe detectors, Nucl. Instrum. Meth. A. 353 (1994) 60, https://doi.org/10.1016/0168-9002(94)91603-9.
[31] A.E. Bolotnikov, N. Abdul-Jabber, S. Babalola, G.S. Camarda, Y. Cui, A. Hossain, E. Jackson, J. James, K.T. Kohman, A. Luryi, R.B. James, Effects of Te inclusions on the performance of CdZnTe radiation detectors, IEEE Trans. Nucl. Sci. 55 (5) (2008) 2757–2764, https://doi.org/10.1109/TNS.2008.2003355.
[32] U.N. Roy, A.E. Bolotnikov, G.S. Camarda, Y. Cui, A. Hossain, K. Lee, M. Marshall, G. Yang, R.B. James, Growth of $CdTe_xSe_{1-x}$ from a Te-rich solution for applications in radiation detection, J. Cryst. Growth 386 (2014) 43–46, https://doi.org/10.1016/j.jcrysgro.2013.09.039.
[33] K. Kim, A.E. Bolotnikov, G.S. Camarda, R. Tappero, A. Hossain, Y. Cui, J. Franc, L. Marchini, A. Zappettini, P. Fochuk, G. Yang, R. Gul, R.B. James, New approaches for making large-volume and uniform CdZnTe and CdMnTe detectors, IEEE Trans. Nucl. Sci. 59 (4) (2012) 1510–1515, https://doi.org/10.1109/TNS.2012.2202917.
[34] U.N. Roy, A. Burger, R.B. James, Growth of CdZnTe crystals by the traveling heater method, J. Cryst. Growth 379 (2013) 57–62, https://doi.org/10.1016/j.jcrysgro.2012.11.047.
[35] E. Kim, Y. Kim, A.E. Bolotnikov, R.B. James, K. Kim, Detector performance and defect densities in CdZnTe after twostep annealing, Nucl. Instrum. Meth. A. 923 (2019) 51–54, https://doi.org/10.1016/j.nima.2019.01.064.
[36] K. Kim, S. Hwang, H. Yu, Y. Choi, Y. Yoon, A.E. Bolotnikov, R.B. James, Two-step annealing to remove Te secondary-phase defects in CdZnTe while preserving the high electrical resistivity, IEEE Trans. Nucl. Sci. 65 (8) (2017) 2333–2337, https://doi.org/10.1109/TNS.2018.2856805.